Automatic Mesh Size Estimation in DVC for Images of Isotropic Materials

Zaira Manigrasso*, Jan Aelterman*, and Wilfried Philips*
*Department Telecommunications and Information Processing
Ghent University, Ghent 900, Belgium
Emails: {Zaira.Manigrasso, Jan.Aelterman, Wilfried.Philips}@UGent.be

***Abstract*—When non-rigid Digital Image Correlation or Digital Volume Correlation (DIC/DVC) is performed, it is critical to correctly set the parameter that determines the control point spacing for the grid on which deformation is defined. In this paper, we present a method to automatically estimate the best performing grid spacing parameter for DIC/DVC registration. The operating principle is that the optimal grid spacing parameter is a function of the image content; it may be estimated through determining the dominant feature/object size. In order to extract the information about the objects size, first, the image volume has been segmented, then the disconnected objects inside the image have been detected (using a labeling technique) and, lastly, a classification of the objects has been made based on the number of the voxels of each object. The reason for this study arises from the practical necessity of finding the best performing parameter for registration in materials sciences research. We show how an erroneous setting of the density of the control points leads to inaccurate registration. Furthermore, we demonstrate how the parameter predicted by our algorithm is indeed optimal, both in a quantitative sense, using Normalized Cross Correlation (NCC) as a measure, as well as qualitatively.**

Keywords–DIC/DVC; B-spline transformation; Grid size estimation.

I. INTRODUCTION

Digital Image Correlation (DIC) and Digital Volume Correlation (DVC) are measurement techniques that make it possible to track 2D and 3D deformations in images. These methods are typically used to obtain the full deformation and strain field [1]. In this paper, we use a DVC global approach, based on B-splines, to estimate non rigid deformations between micro Computer Tomography (micro-CT) 3D images. The deformation is calculated on a regular grid of control points defined by the spacing between the grid nodes. An incorrect choice of grid size negatively impacts not only the final deformation and strain computation [2], but also the computational time, which is linearly related to the number of the grid control points [3].

The displacement between images is characterized by global and local deformation. The global deformation is the perceived direction of the dynamic of the objects. Such direction is the result of a combination of many individual local deformations, and, in the case of non rigid motion, the local deformations have different magnitudes and directions [3][4]. With a coarse grid (large space between the grid nodes), it is only possible to describe global and smooth deformations, however, with a fine grid spacing, it is also possible to describe local and less smooth deformations [3][5]. The use of a coarse grid size is beneficial as it allows to avoid converging to overly non-smooth (and usually incorrect) solutions. By using a finer grid size, the potential to converge to a local optimum increases. The choice of the grid size is usually user dependent, however, self adapting methods have been proposed in order to reduce the dependency of the results on the user's input and in order to improve the deformation and strain accuracy [3][6][7]. These works introduce iterative methods for mesh refining. In [6], the iterative refinement is based on the concept of residual error, instead, in [3] the authors introduce a multi-level approach. For each level, they introduce a control point status associated with each control point, marking it either active or passive. The state is associated with the value of a similarity metric. In [7], the self-adapting algorithm affects the order of the elements of the grid and not their dimensions.

TABLE I. THE BEST PERFORMING GRID SIZE FOR EACH DATASET WITH THE RELATIVE NCC VALUE RESULTED FROM DVC

	Aluminum foam	Leavening dough	Lede stone
Optimal grid size [voxels]	37	22	40
NCC	0.992	0.995	0.991

In this paper, we investigate the idea that, for isotropic materials, the optimal grid size is a function of the image content in a way that the motion of small objects inside the images is better tracked using a fine grid and, vice versa, a coarse mesh can better define the motion of larger objects. Since the B-spline transformation is based on a uniform grid of control points, we tried to link the distance between control points with the most dominant material structure dimension. Our hypothesis is that the most frequently occurring material structure dimension is a good predictor for the optimal grid size in the non rigid DIC/DVC approach. In our study, we applied DVC on six different datasets using a range of different grid size parameters. What has emerged is not only that the estimated deformation field significantly depends on the size parameter, but also that the same grid size is not suitable for all the datasets (Table I).

The rest of the paper is structured as follows. Section II aims to describe the workflow to obtain the optimal grid size spacing for non rigid DIC/DVC. In the Sections III and IV, the details of the DVC experiment and the datasets used are covered, respectively. Results, discussions and conclusion are given in Sections V and VI.

II. PROPOSED METHOD

This method operates from the principle that the optimal grid spacing is a function of the image content. It assumes the characteristic size of the most frequently occurring material structure is indicative of the easiest tracking, as well as the resolution at which deformation can be reliably tracked, and it is, therefore, a good predictor for the optimal grid size in DIC/DVC.

The method consists of 3 steps that are summarized in Figure 1. The purpose of the first step is to segment the objects present in the images in order to measure the size of each of them (Figure 1A). Once the segmentation has been done and the histogram of the objects size

Copyright (c) IARIA, 2020. ISBN: 978-1-61208-791-7

TABLE II. STONE SCANNING SETTINGS

	Lede stone
Acquisition time	48 min
Voxel size	0.02 mm
Volume dimension	1014x1014x752

TABLE III. ALUMINUM FOAM AND LEAVENING DOUGH SCANNING SETTINGS

	Aluminum foam	Leavening dough
Acquisition time	14 min	30 min
Number of gantry rotation	60	75
Number of projection per rotation	700	800
Total compression per rotation	$\pm 133 \mu m$	-
Total compression	$\pm 8 mm$	-
Voxel size	0.02 mm	0.02 mm
Volume dimension	512x512x512	640x640x640

distribution has been created (Figure 1B), the grid size for the image registration is set (Figure 1C). A detailed explanation of each of the 3 steps is provided in the following subsections.

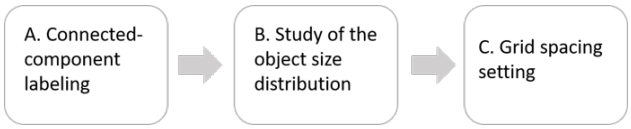

Figure 1. Flowchart of the method.

A. *Connected-component labeling*

Through labeling techniques, we start by distinguishing different disconnected parts of a phase in the image. In micro-CT, these parts represent characteristic small "objects" (e.g., pores, bubbles, nodules). The input of the labeling algorithm is the segmented dataset (binary image), where the voxels belonging to the objects which we want to label are part of the foreground voxels (label = 1) and all other voxels are part of the background (label = 0). The labeling detects each component of foreground voxels and assigns a unique label to all voxels of each object. The labeling algorithm used [8] is based on iterative recursion. The algorithm starts from (0,0,0) voxels and finds the first unlabelled voxel (label = 1) v_1. A cuboid sub-volume is created starting from v_1 and all the voxels inside the volume with label 1 are changed into the label l if they are 26-connected to v_1. For the border voxels of the sub-volume, the procedure done to v_1 is repeated until all the voxels 26-connected to v_1 are marked with l. At the end of the first iteration, the value of the label, l, is incremented by 1 and the algorithm finds the next unlabelled object voxel v_2 and repeats the same procedure done to v_1. The resulted objects are color labeled (different colors for different objects). For each object, its size (in number of voxel) is calculated. Lastly, a histogram that summarizes the number of objects of each size is created.

B. *Study of the object size distribution*

Once the histogram has been created, the dominant object size is taken as a good predictor of the grid spacing: the region

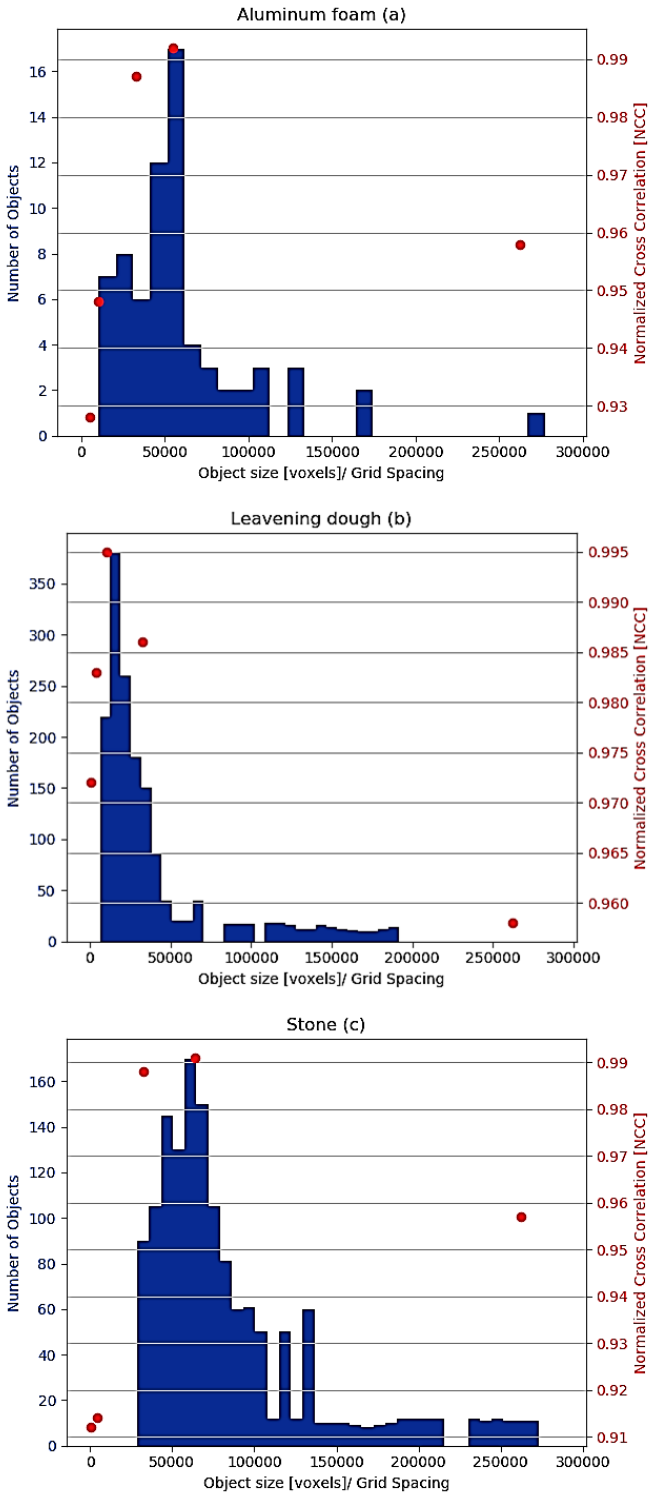

Figure 2. Plot of the registration performance expressed using NCC metric as function of the grid size spacing. On the same graph, the distribution of the objects size inside the image is shown.

around the peak of the histogram is the predicted value for the grid spacing.

C. Grid spacing setting

Since in each dataset there are different structures/objects with different dimensions, it is not possible to match all the structures with an uniform grid, typical of B-spline based DVC. The cells of the grid can be both cubic or rectangular cuboid. For this experiment, cubic cells have been used with the edge length given by the cubic root of the most occurring object size (most numerous class) in voxels.

III. Experimental setup

The experiment has the dual purpose of investigating the influence of the different grid size settings on the deformation estimate and of testing our hypothesis, which is that the optimal grid size setting is related to the most frequently occurring material structure size. The experiment evaluates four different grid sizes, with the length of the edge of the cubic cell given by the powers of 2 (2^3, 2^4, 2^5, 2^6). The registration has also been performed with a cubic cell grid with the edge length equal to the cubic root of the most occurring object dimension inside the dataset. For each registration, the NCC value was calculated in order to compare the results quantitatively.

The chosen transformation is the B-spline. Among the splines functions (e.g., Hermite, plate), B-splines is a popular choice because of its properties of locality, continuity and affine-invariance [9][10]. Because the CT attenuation images are based on the constancy of brightness, NCC is a suitable registration cost function. For minimising it, Adaptative Stochastic Gradient Descent (ASGD) was used [11].

IV. Experimental data

Six different micro-CT 3D datasets were used in this experiment. Three of them are from different materials, exhibiting different dynamics: compression of aluminum foam (Table III), leavening of bread dough (Table III) and water absorption of stone (Lede type) (Table II). To evaluate our claims further, three additional datasets have been created artificially, decreasing the resolution of the previous dataset by a factor of 2 in the 3 dimensions.

The aluminum foam and the leavening dough dataset have been acquired using the Environmental Micro-CT (EMCT) scanner of the Ghent University Centre of X-ray Tomography (UGCT). The Lede stone has been acquired using Tescan CoreTOM. The first two datasets have been acquired during the deformation processes (dynamic scan), whereas the last dataset has been acquired before and after the deformation process (static scan).

V. Results

From the classified data and from their representation by using the histogram, the most dominant object size for each dataset has been extracted. In the case of aluminum foam, the most numerous class, indicating the dimension of the objects inside the image volume, corresponds to 37^3 voxels. To this class belong 18 out of 76 objects (23.68%). Setting the cubic grid size for DVC with the edge length of 37 pixels, the NCC value reaches the peak of 0.992. It is clearly visible in Figure 2: the peak of the metric value coincides with the peak of the classified data. From the histogram, it is visible a range going from $16^3 - 40^3$ where most of the objects belong. The NCC value in this interval is high and decreases significantly for those grid size values for which the number of objects inside the image with the same dimension is low or even null. For the aluminum foam, the worst NCC value corresponds to 8^3 (Figures 2 and 3(a)). In Figure 3, there is a qualitative comparison between the registration with different grid sizes. The most numerous class indicating the dimension

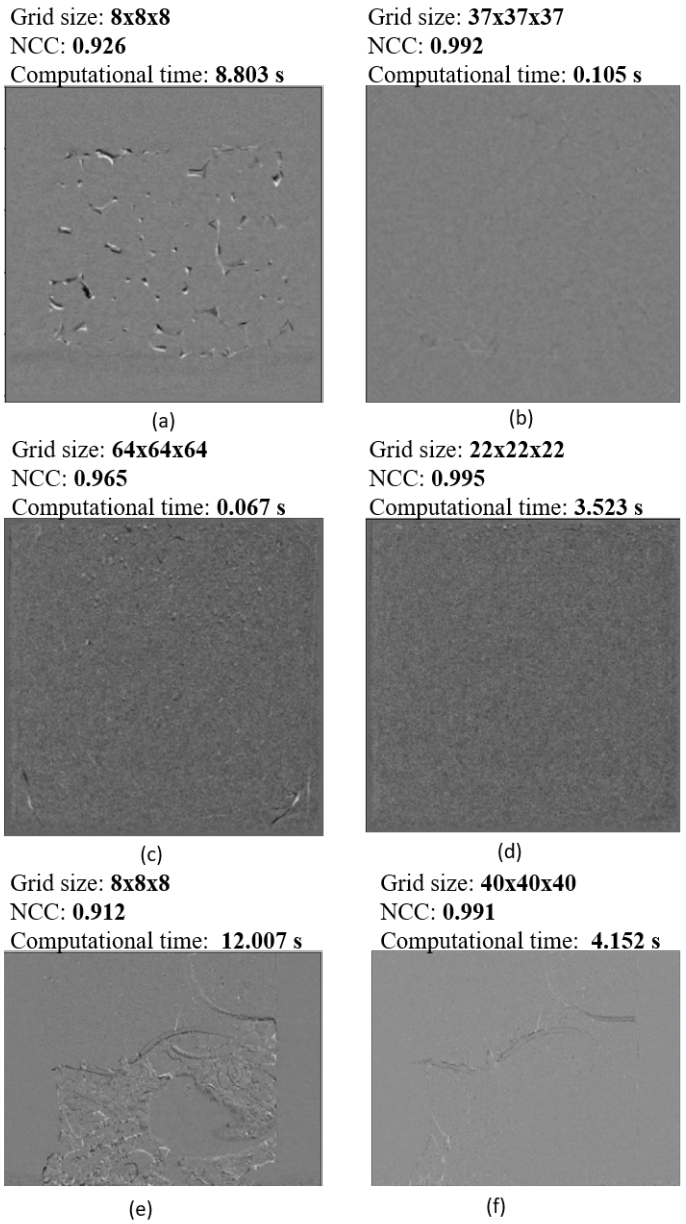

Figure 3. Results of DVC with different grid size settings. (a)-(b): z-y slice of the difference between transformed and reference image of the aluminum foam at full resolution (512x512x512); (c)-(d): z-y slice of the difference between transformed and reference image of the leavening dough at full resolution (640x640x640); (d)-(e): z-y slice of the difference between transformed and reference image of the Lede stone at full resolution (1014x1014x752). The computational time is meant for one DVC iteration.

of the objects for leavening dough and Lede stone are 22^3 and 40^3, respectively. For the leavening dough, most of the objects (73.33%) belong to the interval $15^3 - 30^3$. At the extremes of the range, NCC reaches the vales of 0.983 and 0.985, with a peak of 0.995 in correspondence of the peak of the histogram. For the Lede stone, the most likely interval is $24^3 - 48^3$ with 73.33% , with NCC values at the extremes of the interval of 0.989 and 0.954 and a peak of 0.991 corresponding to the value of grid size of 40^3. As in the case of the aluminum foam, the NCC value decreases considerably if there are no objects which match the grid size. In the case of the leavening dough, the worst registration result has been obtained with the grid cell dimension of 64^3 (NCC = 0.965) (Figure 3(c)), followed by the result obtained with the grid size of 8^3 (NCC = 0.975) (Figure 2). The Lede stone dataset has low NCC value for grid sizes of 8^3 (NCC=0.912) and 16^3 (NCC=0.913) (Figure 2 and 3).

To have more evidence about the validity of the proposed method, the same experiment has been repeated on the same datasets at lower resolution. The resolution has been decreased by a factor of 2 along the three dimensions. According to our hypothesis, the optimal value of the grid size should be different from the previous value on the full resolution dataset. Since the resolution has been decreased by a factor of 2, the dimensions of the objects/structures inside the image are also smaller and, therefore, the optimal distances between the nodes of the grid are reduced by a factor of 2. The results of the experiment are reported in Figure 4.

VI. Conclusion

The study carried out in this paper confirms our initial hypothesis: the best performing value for the grid spacing parameter is linked to the most occurring material structure size. The advantage of this method compared with other techniques present in literature [3][6][7] is that it is able to give to the user prior information about the optimal grid size ready to be used in many of the open source libraries and commercial software for DVC.

With this research, we are not suggesting that this parameter optimization method is globally optimal, instead, we suggest that it may be a practically useful heuristic to automate DVC/DIC algorithms. Indeed, in a purely theoretical sense, the optimal grid size decision should additionally depend on the kinematics of the material sample, not just its structural makeup. In this study, the nature of the deformation is not taken in consideration, as it could be argued that it is unrealistic anyhow to expect software to track motion fields that are erratic on a finer resolution scale than the finest resolution of the visible structures.

With this study, we are able to give some guidelines for the setting of the optimal grid spacing parameter for DVC/DIC in order to be less user dependent. Furthermore, being an automated method, it is possible to integrate it in a future software for DVC.

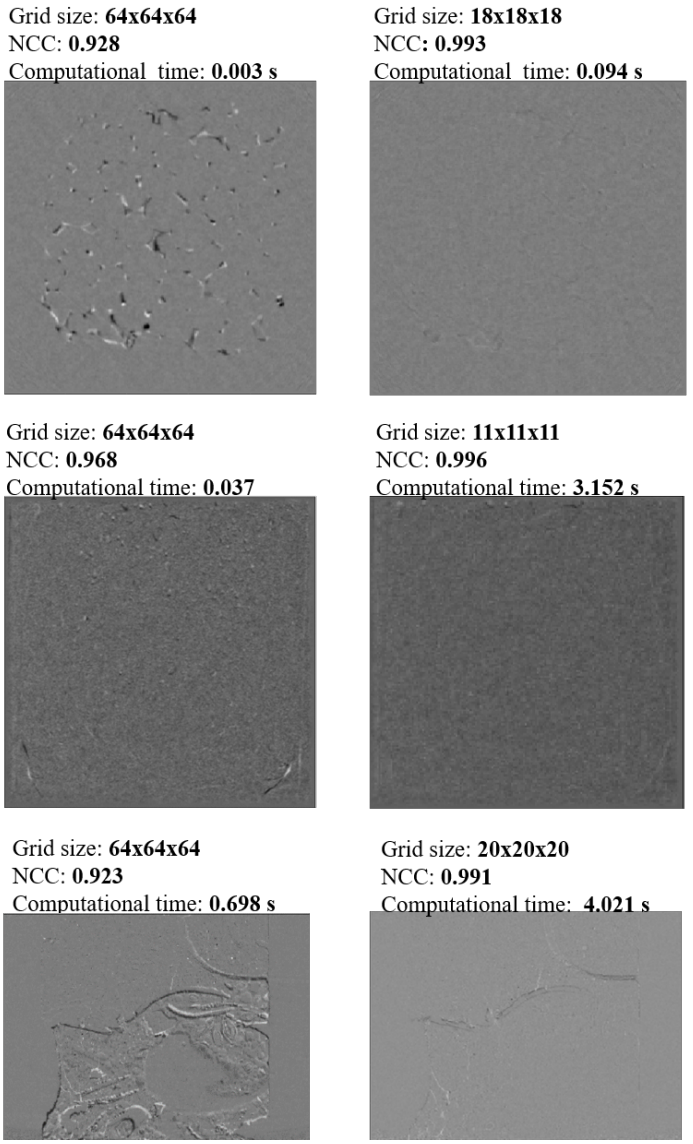

Figure 4. Results of DVC with different grid size settings. (a)-(b): z-y slice of the difference between transformed and reference image of the aluminum foam at half resolution (256x256x256); (c)-(d): z-y slice of the difference between transformed and reference image of the leavening dough at half resolution (320x320x320); (d)-(e): z-y slice of the difference between transformed and reference image of the Lede stone at half resolution (507x507x376).The computational time is meant for one DVC iteration.

Acknowledgment

This work was funded by the Research Foundation — Flanders in the Strategic Basic Research Programme (FWO-SBO), file number S003418N. The authors thank UGCT (UGent, Centre for X-ray Tomography) for the aluminum foam and leavening dough dataset, Dr. Tim De Kock (FWO post doctoral research fellow at the time of the acquisition) and TESCAN-XRE for the dataset of Lede stone.

References

[1] B. Bay, T. Smith, D. Fyhrie, and M. Saad, "Digital Volume Correlation: Three-dimensional Strain Mapping Using X-ray Tomography ," Experimental Mechanics, vol. 39, 1999, pp. 217–226.

[2] F. Mortazavi, "Development of a global digital image correlation approach for a fast high-resolution displacement measurements," PhD thesis, École Polytechnique de Montréal., 2013.

[3] J. Schnabel, "A generic Framework for Non-Rigid Registration Based on Non-uniform Multi-level free-Form Deformations," Medical Image Computing and Computer-Assisted Intervention – MICCAI, 2001, pp. 573–581.

Copyright (c) IARIA, 2020. ISBN: 978-1-61208-791-7

[4] S. Klein, M. Staring, K. Murphy, M. Viergever, and J. Pluim, “elastix: a toolbox for intensity based medical image registration,” IEEE Transactions on Medical Imaging, vol. 29, 2010, pp. 196–205.

[5] L. Zhang, M. Li, and F. P. Hou, W., “Registration of Lung CT Images Using B-spline Based Free-Form Deformation,” IEEE International Conference on Progress in Informatics and Computing (PIC), 2018.

[6] X. Wang and S. Ma, “Mesh-Based Digital Image Correlation Method Using Non-Uniform Elements for Measuring Displacement Fields with High Gradient,” Experimental Mechanics, vol. 54, 2014, pp. 1545 – 1554.

[7] L. Wittevrongel, S. Lava, P. Lomov, and D. Debruyne, “A Self Adaptive Global Digital Image Correlation Algorithm,” Experimental Mechanics, vol. 55, 2014, pp. 361–378.

[8] Q. Hu, G. Qian, and W. Nowinski, “Fast connected-component labelling in three-dimensional binary images based on iterative recursion,” Computer Vision and Image Understanding, vol. 99, 2005, pp. 414–434.

[9] L. Piegl and W. Tiller, The NURBS book. Springer Science Business Media, 1996.

[10] Y. Yin, E. Hoffman, and C. Lin, “Mass preserving nonrigid registration of CT lung images using cubic B-spline,” Medical Physics, vol. 36, 2009, pp. 4213–4222.

[11] S. Klein, J. Pluim, M. Staring, and M. Viergever, “Adaptive stochastic gradient descent optimisation for image registration ,” International journal of Computer Vision, vol. 81, 2009, pp. 227–239.

Copyright (c) IARIA, 2020. ISBN: 978-1-61208-791-7